Solvent effects in grafting-through ring-opening metathesis polymerization

*Sarah E. Blosch, Mohammed Alaboalirat, Cabell B. Eades, Samantha J. Scannelli, John B. Matson**

Department of Chemistry and Macromolecules Innovation Institute, Virginia Tech, Blacksburg, Virginia, 24061, United States

KEYWORDS: Bottlebrush polymer, graft polymer, macromonomer, propagation, rate, kinetics, purity

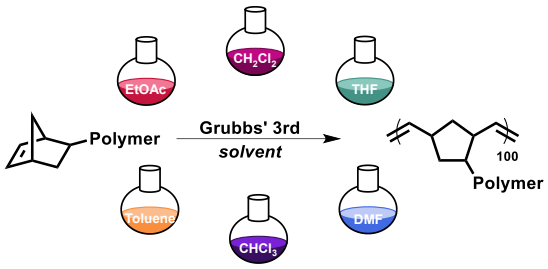

For Table of Contents use only

ABSTRACT

Ring-opening metathesis polymerization (ROMP) utilizing Grubbs' third-generation catalyst ($(H_2IMes)(Cl)_2(pyr)_2RuCHPh$) shows characteristics of living polymerizations, including molecular weights increasing with monomer conversion and the ability to make (multi)block copolymers. However, irreversible termination reactions still occur due to catalyst decomposition, leading to terminated chains, especially in the context of sterically demanding monomers such as macromonomers (MM). In this work, we performed identical ROMP reactions on three different MMs in six solvents commonly used in ROMP with varying levels of purity. The solvents included ethyl acetate (EtOAc), dichloromethane (CH_2Cl_2), chloroform ($CHCl_3$), toluene, tetrahydrofuran (THF), and *N,N*-dimethylformamide (DMF). All polymerizations were conducted under air targeting a bottlebrush polymer backbone degree of polymerization (N_{bb}) of 100. All three MMs included a norbornene on the α chain end and had molecular weights (M_n) of ~4 kg/mol. They included one polystyrene MM with a bromine on the ω chain end and two poly(*n*-butyl acrylate) MMs with either a bromine or a trithiocarbonate group on the ω chain end. Solvent choice, and in some cases level of purity, led to significant differences in the propagation rate in these ROMP grafting-through reactions. Of the solvents tested, propagation rates in EtOAc and CH_2Cl_2 were approximately 4-fold and 2-fold faster, respectively, than $CHCl_3$, toluene, and THF for all MMs. Propagation was much slower in DMF for the polystyrene MM than all the other solvents, and on par with the slower solvents for the two poly(*n*-butyl acrylate) MMs tested. The purity of the solvent in some cases had a profound effect on the propagation rate: In the case of EtOAc, purification led to a 2-fold decrease in propagation rate; in contrast, purification of THF was required to observe full conversion of MM to bottlebrush polymer. The functional group on the ω chain end did not influence the rate of ROMP. Utilizing UV-Vis spectroscopy to measure catalyst

decomposition, the main polymer termination route in ROMP, we uncovered dramatic solvent effects, where the catalyst decomposed over ten times faster in THF and DMF than in toluene. Finally, studies targeting N_{bb} = 500 or 1000 revealed that toluene, EtOAc, and CH_2Cl_2 demonstrated the highest degree of "livingness" in ROMP. These results will enable the synthesis of complex polymer architectures using ROMP with a high degree of living character.

INTRODUCTION

Ring-opening metathesis polymerization (ROMP) has become a powerful tool for polymer synthesis, especially in constructing complex polymer architectures (i.e., topologies).[1,2] High strain, cyclic olefin monomers combined with the fast-initiating catalyst $(H_2IMes)(Cl)_2(pyr)_2RuCHPh$ (Grubbs' third-generation catalyst, G3) are widely used in ROMP,[3] but catalyst decomposition (also called catalyst death or catalyst degradation), even at a slow rate, leads to irreversible termination, preventing classification as a living polymerization.[4] ROMP, nonetheless, can have low enough rates of termination that it often exhibits the characteristics of living polymerizations, including molecular weights that increase linearly with conversion and the possibility for chain extension to make block copolymers. These traits enable the synthesis of well-defined polymers using a variety of monomers containing a large breadth of functional groups with precise topologies, such as star polymers,[5–8] hyperbranched polymers,[9–11] single chain nanoparticles,[12–14] polymers with bulky side chains,[15–18] and densely grafted bottlebrush (BB) polymers,[19–21] among others. However, in particularly challenging polymerizations, including ROMP of monomers with large substituents or synthesis of multiblock copolymers, termination via catalyst decomposition can lead to broader than expected molecular weight distributions and/or mixtures of products. Many experimental factors influence the efficiency of ROMP in the synthesis of complex polymer topologies, and despite widespread use of this polymerization

method, studies are remarkably lacking on how reaction parameters such as solvent influence ROMP.

Solvent effects in olefin metathesis have been studied in small molecule reactions such as ring-closing metathesis,[22–24] acyclic diene metathesis (ADMET) polymerization,[25] and ROMP, focusing mostly on initiation rates or using catalysts other than G3.[26–31] For example, Thompson and coworkers found that when performing ROMP using noble metal halide catalysts, solvents that can complex to the propagating species via hydrogen bonding or via Lewis acid/Lewis base interactions resulted in dramatic changes in the tacticity of the polymer products and in the reactivity ratios in copolymerizations.[31] In ADMET, Schulz and Wagener showed that solvent choice greatly affected the maximum molecular weight achievable, with molecular weights almost an order of magnitude higher in dichloromethane (CH_2Cl_2) than the same polymerization performed in tetrahydrofuran (THF).[25] They concluded that the rate of catalyst decomposition played the most significant role in achieving high molecular weights. However, to our knowledge no systematic solvent studies have been reported for ROMP using the fast-initiating and widely used G3 catalyst.

We sought to evaluate how common organic solvents affect the rate of propagation (k_p) and the rate of termination (k_t) in ROMP. Knowledge of both rates is critical because the k_p/k_t ratio is the primary factor influencing the "livingness" of a particular polymerization.[32] Small molecule monomers can be investigated to determine these effects; however, knowledge of solvent effects on rates is more important for larger macromonomers (MMs) because k_p decreases as the molar mass of the MM increases,[33] decreasing the k_p/k_t ratio and the degree of "livingness". MMs with even moderate molecular weights can lead to low polymer backbone degrees of polymerization (DP) in the grafting-through step due to the steric hindrance around the propagating site.[34–36]

Beyond BB polymers, both a high k_p and a high k_p/k_t ratio are critical for any ROMP reaction with sterically demanding pendant groups (e.g., sugars, peptides, dendrons), side chains requiring specific solvents (e.g., polar side chains), or even in the synthesis of high molecular weight linear homopolymers and block copolymers.

Herein we aimed to compare propagation rates in the ROMP of various MMs in six organic solvents commonly used in ROMP and other olefin metathesis reactions. These include ethyl acetate (EtOAc), CH_2Cl_2, chloroform ($CHCl_3$), toluene, THF, and *N,N*-dimethylformamide (DMF). Additionally, we varied the purification methods for each solvent, while also investigating three different MMs with varied side chain structures and/or end groups. In all cases, we conducted ROMP reactions in capped vials under air rather than in a glovebox in order to measure solvent effects under these minimally stringent and widely used conditions. We hypothesized that solvent type and purification method would affect both k_p and k_t in ROMP and thus influence the "livingness" of the polymerization. Ultimately, we envisioned that these results would guide researchers in choosing the optimal solvent to synthesize well-defined polymers using ROMP.

EXPERIMENTAL

Materials

All reagents were obtained from commercial vendors and used as received unless otherwise stated. The six solvents used in the study were EtOAc (VWR BDH Chemicals, ACS grade, ≥99.5%) CH_2Cl_2 (Fischer, certified ACS grade, ≥99.5%), $CHCl_3$ (Fischer, HPLC grade, ≥99.5%), toluene (Fischer, ACS grade, ≥99.5%), THF (Fischer, HPLC grade, ≥99.9%, uninhibited), and DMF (Fischer, HPLC grade, ≥99.7%). Toluene and THF were stored on a column of activated alumina under nitrogen in a solvent purification system (MBraun). *Exo*-norbornene-methanol was prepared as described previously.[37] G3 catalyst was prepared as previously described.[28,38] Each

batch of G3 was only used for 48 h after synthesis due to observations of lower conversions if used after this period of time.

Characterization

Size-exclusion chromatography (SEC) was performed in THF containing 0.025 wt% butylated hydroxytoluene (BHT) at a rate of 1 mL/min at 30 ºC, on two MIXED-B Agilent PLgel 10 μm columns connected in a series with a Wyatt Optilab Rex refractive index detector and a Wyatt Dawn Heleos 2 multi-angle light scattering detector. UV-Vis measurements were performed using a Cary 60 UV-Vis and fiber optic dip probe. NMR spectroscopy was performed using an Agilent 400 MHz spectrometer with spectra referenced to internal solvent resonances.

Synthesis of *exo*-norbornene-methyl 2-bromo-2-methylpropanoate (**NBMP**)

The norbornene-functionalized atom transfer radical polymerization (ATRP) initiator, **NBMP**, was synthesized according to the procedure reported in a recent study (Scheme S1).[37] NMR spectra were consistent with literature reports. ^{1}H NMR ($CDCl_3$): δ 6.16 (m, 1H), 5.95 (m, 2H), 4.72 (m, 1H), 2.92 (s, 1H), 2.87 (s, 2H), 1.90 (s, 3H, CH_3), 1.75-1.42 (m, 10H). ^{13}C NMR ($CDCl_3$): δ 171.6, 141.6, 132.4, 76.9, 56.3, 47.7, 47.1, 46.4, 45.7, 42.3, 40.7, 34.5, 34.4, 30.8, 30.7.

Synthesis *exo*-norbornene-methyl 2-(((dodecylthio)carbonothioyl)thio)-2-methylpropanoate **(NDTMP)**:

The norbornene-functionalized photoiniferter, **NDTMP**, was synthesized according to the procedure reported in a recent study (Scheme S2).[37] NMR spectra were consistent with literature reports. ^{1}H NMR ($CDCl_3$): δ 6.07 (m, 2H), 4.22 (dd, J = 10.8 Hz, 6.4 Hz, 1H), 3.95 (dd, J = 10.8 Hz, 9.2 Hz, 1H), 3.27 (td, J = 7.4 Hz, 2.1 Hz, 2H), 2.82 (s, 1H), 2.66 (s, 1H), 1.70 (s, 6H), 1.31 (m, 3H), 1.25 (m, 20H), 0.88 (t, J = 7 Hz, 3H). ^{13}C NMR ($CDCl_3$): δ 221.6, 173.2, 137.0, 136.5,

70.2, 56.2, 45.1, 43.8, 41.8, 37.9, 37.0, 32.1, 29.8, 29.7, 29.6, 29.5, 29.3, 29.1, 28.1, 25.6, 25.6, 22.9, 14.3.

Synthesis of **PS_{Br}**:

A polystyrene MM containing a Br end group (**PS_{Br}**) was synthesized using atom-transfer radical polymerization (ATRP). Styrene (30 mL, 358 equiv, 262 mmol) was added to an oven-dried 100 mL Schlenk tube containing a magnetic stir bar, followed by **NBMP** (0.20 g, 1 equiv, 0.73 mmol), CuBr (52 mg, 0.5 equiv, 0.37 mmol), and $CuBr_2$ (82 mg, 0.5 equiv, 0.37 mmol). The mixture was deoxygenated using three freeze-pump-thaw cycles, then heated in a 90 °C oil bath for ~10 min before *N,N,N',N'',N''*-pentamethyldiethylenetriamine (PMDETA) (0.15 mL, 1 equiv, 0.73 mmol) was added via syringe. The reaction mixture was allowed to stir for 3 h, then the Schlenk tube was removed from the oil bath, and the valve was removed to expose the contents to air to terminate the reaction. The MM was then purified and isolated by adding approximately 150 mL EtOAc and washing with 150 mL of water in a separatory funnel. The organic layer was then washed with brine (150 mL) and dried over $MgSO_4$. The EtOAc was removed by rotary evaporation, and the resulting clear, viscous solution was dissolved in approximately 50 mL of CH_2Cl_2.Next, this solution was precipitated by dropwise addition to 1 L of stirring CH_3OH. The solid was recovered by filtration, redissolved in CH_2Cl_2, and precipitated again. This precipitation process was performed three times in total with the final white solid recovered by filtration and dried overnight, yielding 2.8 g **PS_{Br}** (Scheme S3). The molecular weight was estimated using end-group analysis by ^{1}H NMR spectroscopy and found to be 4400 g/mol (Figure S1), and by SEC and found to have a number average molecular weight (M_n) of 4500 g/mol and $Đ$ = 1.03 (Figure S2).

Synthesis of **PnBA$_{Br}$**:

ATRP was used to synthesize a poly(*n*-butyl acrylate) MM containing a Br end group (**PnBA$_{Br}$**). CuBr (26 mg, 0.5 equiv, 0.18 mmol), **NBMP** (0.10 g, 1 equiv, 0.37 mmol), *n*-butyl acrylate (4.0 mL, 75 equiv, 27 mmol), and acetone (1.4 mL) were added to an oven-dried 100 mL Schlenk tube containing a magnetic stir bar. The Schlenk tube was deoxygenated by three freeze-pump thaw cycles and backfilled with N_2. The reaction mixture was stirred at 60 ºC for ~10 min before PMDETA (0.15 mL, 0.5 eq, 0.18 mmol) was added via syringe, and then the mixture was heated and stirred for 12 h. The Schlenk tube was removed from the oil bath, and the valve was removed to expose the contents to air to terminate the reaction. An aliquot was removed for analysis of monomer conversion; ^{1}H NMR spectroscopy showed 48% conversion of *n*-butyl acrylate to poly(*n*-butyl acrylate). The MM was then purified and isolated by adding approximately 150 mL EtOAc and washing with 150 mL of water in a separatory funnel. The organic layer was then washed with brine (150 mL) and dried with $MgSO_4$. The EtOAc was removed via rotary evaporation, and the residual *n*-butyl acrylate was removed by adding around 20 mL DMF and drying by blowing air overnight. The crude product was then dissolved in around 100 mL THF and passed through basic alumina. The THF was removed by rotary evaporation, and the semi-translucent, viscous liquid was dried under vacuum yielding 1.3 g of **PnBA$_{Br}$** with an expected molecular weight (by conversion) of 4700 g/mol (Scheme S4). The molecular weight was estimated using end-group analysis by ^{1}H NMR spectroscopy and found to be 4000 g/mol (Figure S4) and by SEC and found to have an M_n of 4200 g/mol and $Đ$ of 1.14 (Figure S5).

Synthesis of **PnBA$_{TTC}$**:

The synthesis of the **PnBA$_{TTC}$** MM utilized photoiniferter polymerization using a photoreactor similar to that previously reported.[39] *n*-Butyl acrylate (3.4 mL, 50 equiv, 23.4 mmol) was passed through three basic alumina plugs, then added to an oven-dried 100 mL Schlenk tube containing a magnetic stir bar, along with **NDTMP** (168 mg, 1 equiv, 0.47 mmol) 2,2'-azobis(2-methylpropionitrile) (AIBN) (0.77 mg, 0.01 equiv, 4.7 μmol), and THF (13.4 mL). The mixture was deoxygenated by five freeze-pump-thaw cycles before being placed into the photoreactor containing a blue LED light (λ = 450 nm) and stirred for 6.5 h at room temperature. The Schlenk tube was removed from the reactor, and the valve was removed to expose the contents to air to terminate the reaction. An aliquot was removed for analysis of monomer conversion; ^{1}H NMR spectroscopy showed 47% conversion of *n*-butyl acrylate to poly(*n*-butyl acrylate). The excess nBA and THF were removed from the mixture by adding around 20 mL DMF and overnight evaporation by blow-drying with air, followed by overnight drying under vacuum yielding 1.6 g of a yellow, viscous liquid with an expected molecular weight, based on conversion, of 3300 g/mol (Scheme S5). The molecular weight was estimated using end-group analysis by ^{1}H NMR spectroscopy and found to be 3900 g/mol (Figure S7) and by SEC and found to have an M_n of 3900 g/mol and $Đ$ of 1.10 (Figure S8).

Synthesis of **NMB**:

A small molecule norbornene, *exo*-norbornene-5-methyl benzoate (**NMB**), was prepared using 1-ethyl-3-(3-dimethylaminopropyl)carbodiimide (EDC) coupling (Scheme S6). *Exo*-norbornene-methanol (1.0 g, 8.05 mmol) and EDC (1.63 g, 10.5 mmol) were dissolved in CH_2Cl_2 (25 mL) in a round bottom flask equipped with a stir bar. The contents were stirred until the solids had completely dissolved (~5 min). A second flask was charged with benzyl alcohol (1.28 g, 10.5

mmol), *N,N*-dimethylpyridin-4-amine (DMAP) (0.492 g, 4.03 mmol), and 25 mL CH_2Cl_2. This second solution was added dropwise into the flask containing *exo*-norbornene-methanol while stirring. After complete addition, the reaction mixture was stirred at room temperature for 12 h, monitoring conversion by TLC with CH_2Cl_2 as the mobile phase and a potassium permanganate stain. The reaction mixture was transferred to a separatory funnel and washed three times with saturated sodium carbonate and once with brine, dried over sodium sulfate, and concentrated by rotary evaporation. The concentrated crude product was purified by a silica column, eluting with 5% EtOAc in hexanes. The product was obtained as a colorless oil (0.96 g, 52% yield). ^{1}H NMR ($CDCl_3$): δ 8.11–8.02 (m, 2H), 7.60–7.53 (m, 1H), 7.49–7.40 (m, 2H), 6.12 (m, 2H), 4.42 (m, 1H), 4.22 (m, 1H), 2.91–2.78 (m, 2H), 1.96–1.83 (m, 1H), 1.45–1.22 (m, 5H). ^{13}C NMR ($CDCl_3$): δ 166.38, 136.72, 135.98, 132.58, 130.21, 129.31, 128.08, 68.74, 44.75, 43.46, 41.37, 37.84, 29.33. Both ^{13}C and ^{1}H NMR spectra match literature values.[40]

Purification methods for solvents

Three different purity conditions were used to test the effects of potential impurities in each solvent. The "as received" solvents were obtained from commercial vendors (specific vendor and grade are highlighted in the materials section) and used straight from the bottle. The "distilled" solvents were distilled at atmospheric pressure, except for DMF which was distilled at reduced pressure, and stored in an inert atmosphere over 3 Å molecular sieves. The "purified" solvents were purified either using solvent purification columns or following detailed procedures from *Purification of Laboratory Chemicals.*[41] These methods are as follows:

EtOAc was purified by washing with equal volumes of saturated aqueous sodium carbonate in a separatory funnel, followed by brine, before removing the organic layer and drying over $MgSO_4$.

The solvent was then distilled onto molecular sieves and was stored in a Strauss flask under nitrogen protected from the light. CH_2Cl_2 was first shaken with portions of concentrated sulfuric acid (around 15 mL per 200 mL of CH_2Cl_2) in a separatory funnel until the slightly yellow H_2SO_4 layer turned and remained colorless. The solvent was then washed with water in a separatory funnel, then washed with 5 w/v % NaOH in water, followed by a final wash with water. The CH_2Cl_2 was then dried over $MgSO_4$ and stirred with 10 w/v % $CaCl_2$ overnight. The solution was filtered to remove $CaCl_2$ and then distilled from 10 w/v % $CaSO_4$ onto molecular sieves. The purified solvent was stored on sieves in a nitrogen-filled Strauss flask protected from the light. $CHCl_3$ was washed with water using a separatory funnel before drying over 5 w/v% $CaCl_2$ for 3 h. The $CaCl_2$ was filtered off, fresh $CaCl_2$ (5 w/v %) was added, and the solution was refluxed for 4–6 h. The solution was filtered, then distilled onto molecular sieves and was stored in a Strauss flask under nitrogen protected from the light. DMF was stirred over 5 w/v % CaH_2 overnight, then filtered. The DMF was then distilled at reduced pressure onto molecular sieves and was stored in a Strauss flask under nitrogen protected from the light. Both toluene and THF were taken from solvent drying columns charged with activated alumina and used immediately after removal from the column.

Evaluation of propagation rates of MMs

A representative method for the ROMP of each MM under air is as follows: The MM (40 mg, 100 equiv, 8.9 μmol) was added to a 1-dram vial at a concentration of 50 mg/mL in the chosen solvent. Grubbs' third generation catalyst (G3, 2.0 mg) was dissolved in 0.9 mL of the solvent, and 30 μL of the solution was added rapidly to the stirring MM solution via a 100 μL syringe at a molar ratio of 100:1 MM:G3. The vial was capped, and at specific timepoints throughout the

polymerization, 50 μL aliquots were removed via syringe and added to vials containing a few drops of ethyl vinyl ether (EVE) to terminate the reaction. The solutions were allowed to dry by leaving the vials open to the air overnight, then the residual solids were dissolved in THF for SEC analysis to measure MM conversion to BB polymer, molecular weight, and *Đ*. This process was repeated in triplicate for each solvent type and level of purity for **PS$_{Br}$**, and for each pure solvent for **PnBA$_{Br}$** and **PnBA$_{TTC}$**.

Kinetic Analysis of BB Polymers by SEC

To determine conversion, molecular weight, and dispersity at each timepoint during the polymerization of **PS$_{Br}$**, **PnBA$_{Br}$**, and **PnBA$_{TTC}$**, samples were prepared for analysis by SEC. The dried polymer mixture, taken at each timepoint during the course of the reaction, was dissolved in 1 mL THF inhibited by 0.025 wt% butylated hydroxytoluene (BHT) and filtered into an SEC vial and analyzed by SEC. Molecular weights were obtained using a d*n*/d*c* value of 0.185 and 0.074 for PS and PnBA, respectively. Polymerization conversion was measured by comparing the relative integrations of the MM and BB polymer peaks in the RI traces using these d*n*/d*c* values for both peaks. Propagation rate constants and half-lives were calculated by fitting conversion data to a first-order kinetics plot. A maximum conversion of less than 100% was used for each of the MMs (94% for **PS$_{Br}$**, 90% for **PnBA$_{Br}$**, and 88% for **PnBA$_{TTC}$**) due to a small amount of the MM lacking a norbornene functional group, as we have seen previously in MMs prepared using reversible-deactivation radical polymerization (RDRP) methods.[39,42] SEC traces for polymerization of each MM in each solvent with different purities, as well as the rate graphs, can be found in the SI (Figures S10-S33).

Kinetics of ROMP of **NMB**

Small molecule norbornene, **NMB**, was polymerized via ROMP, and the kinetics were determined using ^{1}H NMR spectroscopy. A representative procedure is as follows: **NMB** (40 mg, 100 equiv, 181 μmol) was added to a scintillation vial containing a magnetic stir bar and enough solvent for a 20 mM concentration (8.8 mL). A solution of pyridine was created by adding 0.2 mL pyridine to 1.4 mL of the chosen solvent and injecting 10 μL into the **NMB** solution (final amount added was 1.5 μL, 10 equiv, 18 μmol). A G3 solution was made by adding 2.5 mg of G3 into 0.12 mL of solvent, then a portion of this solution (60 μL, final amount added of solution was 1.28 mg, 1 equiv, 1.8 μmol) was injected rapidly via syringe into the stirring **NMB** solution to make a final reaction mixture containing 100 equiv NMB, 10 equiv pyridine, and 1 equiv G3. Several 500 μL aliquots were taken throughout the 20 min polymerization and added into vials containing a few drops of EVE. The resulting solutions were allowed to air dry for 24–48 h before dissolving in $CDCl_3$ and analyzing using ^{1}H NMR spectroscopy (16 scans, 2 s relaxation delay). Monomer conversion was determined by integrating the norbornene olefin proton peaks (around 6.2 ppm) and the norbornene polymer peaks (broad peak around 5.2 ppm) (Figure S34) and comparing the polymer proton peaks' integration values to the integration value of protons. Half-life values were calculated from first-order kinetics fits using these conversions.

Tracking catalyst decomposition via UV-Vis

To monitor catalyst decomposition over time, a fiber optic dip probe was attached to the UV-Vis spectrometer. G3 was dissolved in solvent at a concentration of 0.075 mg/mL at a volume of around 10–12 mL in a 20 mL scintillation vial containing a magnetic stir bar. The vial was placed onto a stir plate, the dip probe was inserted into the vial, and parafilm was wrapped around the top of the vial to limit evaporation of the solvent. Spectra were collected from 250 to 500 nm (2 nm

step) every 30 sec with timepoints starting approximately 5–10 seconds after the G3 was added to the solvent (lamp crossover was set to 350 nm). This was repeated in triplicate for each of the six pure solvents. To accurately determine rate constants for each solvent, the decomposition profiles were normalized to the maximum absorption for each sample at 344 nm, and a first-order kinetic analysis was applied (see Figures S35-S40 and discussion in the SI for details).

RESULTS AND DISCUSSION

BB polymers contain a polymer backbone with pendant polymer side chains that can take on various shapes depending on pendant chain grafting density and chemistry, backbone chemistry, and the DPs of both (N_{bb} and N_{sc}, respectively). The grafting-through synthetic method allows for the best control over grafting density uniformity, allowing for "perfect" grafting density. This is achieved by polymerizing an MM, which is a homotelechelic polymer containing a polymerizable group (e.g., a norbornene) on one chain end.[43] This "perfect" grafting density is important because it significantly affects the conformation of the polymer, causing backbone chain extension and essentially eliminating entanglements within the pendant chains and between BB polymers.[44] The unique properties and topologies of BB polymers make them an exciting topic in polymer science that has gained attention in the past few decades as nanoscale materials with unique shapes and properties that can be applied as drug delivery agents,[45–48] photonic crystals,[49–52] interfacially active agents,[53–55] nanomaterials with tunable sizes and shapes,[56,57] and in the creation of elastomers with unique properties.[58–60] Likewise, synthesizing BB polymers enables further understanding of the ideal reaction conditions in ROMP.

Our laboratory, along with others, has sought to create large, well-defined BB polymers, some with unique architectures such as tapered BB polymers.[37,42,61,62] In these efforts we aim to optimize "livingness" in ROMP to achieve well-defined, low $Đ$ polymers. In 2016 we discovered that the

choice of anchor group, the series of atoms connecting the norbornene to the polymer chain in an MM, significantly affects the rate of propagation in ROMP.[34] We have also noticed that the choice of solvent affects the propagation rate in ROMP, as well as the maximum conversion that can be achieved during the synthesis of BB polymers. While anecdotal mentions of solvent effects in ROMP in the context of complex polymer topologies have appeared in a few papers from our group and others,[34,42,63] no systematic studies have been conducted. In addition to differences in propagation rates depending on solvent choice, we have also observed that the method of purification of the chosen solvent can sometimes make a difference in the efficiency of ROMP. Here we set out to systematically study these phenomena.

Solvent type and purity effects on ROMP propagation rate

To investigate the effect that solvent choice and purity have on the propagation rate of ROMP, we first employed ATRP to synthesize a polystyrene MM on the 3 g scale (**PS$_{Br}$**) with an M_n of 4500 g/mol (N_{sc} = 40) and a $Đ$ of 1.03 (Scheme 1). We targeted an M_n of less than 5000 g/mol because we have observed a substantial decrease in monomer conversion if N_{sc} exceeds ~50. This batch of **PS$_{Br}$** MM was used throughout the entirety of this portion of the study to measure k_p for six solvents with differing levels of purity.

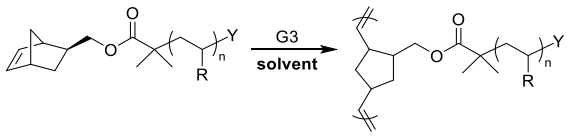

PS$_{Br}$: R = Ph, Y = Br (M_n = 4500 g/mol, $Đ$ = 1.03)
PnBA$_{Br}$: R = C(O)OnBu Y = Br (M_n = 4200 g/mol, $Đ$ = 1.14)
PnBA$_{TTC}$: R = C(O)OnBu Y = SC(S)SC$_{12}$H$_{25}$ (M_n = 3900 g/mol, $Đ$ = 1.10)

Scheme 1. Representative scheme of the grafting-through ROMP of the three MMs used in this study.

We chose six solvents based on their wide use in ROMP: EtOAc, CH_2Cl_2, $CHCl_3$, toluene, THF (uninhibited), and DMF. We hypothesized that purification of each solvent might increase k_p by removing impurities that could hinder the activity of the catalyst. To investigate purification effects on k_p, we used three different categories of purification. The first was the "as received" category, in which we took the solvent directly from the bottle. The second and third categories involved performing simple distillations as well as more rigorous purifications for each solvent, which we term "distilled" and "purified," respectively. In this third category, each solvent was purified either by passage through solvent purification columns or by following procedures outlined in *Purification of Laboratory Chemicals,*[41] as discussed in the experimental section.

To experimentally measure $k_{p,obs}$, we polymerized $\mathbf{PS_{Br}}$ MM with a ratio of 100:1 MM:G3 (i.e., target $N_{bb} = 100$), at a concentration of 50 mg/mL in each solvent (Scheme 1). Reactions were performed in capped vials under air at room temperature. Aliquots were removed at pre-determined timepoints and added to vials containing EVE to terminate the polymerization. Solvents were removed, then MM conversion and molecular weight at each timepoint were determined via SEC analysis by comparing the integrations of the MM and BB polymer peaks using the known d*n*/d*c* value for polystyrene in THF (0.185 mL/g) for both. After plotting conversion versus time using these experimental conversion results, the data were fitted to a first-order kinetic model, from which $k_{p,obs}$ values were determined. Each polymerization of $\mathbf{PS_{Br}}$ was performed three to four times in each of the different solvents (six solvents with three different purification methods each).

First-order kinetics fits are shown in Figure 1A for a representative solvent (CH_2Cl_2) for all three purity levels. Similar graphs for the other five solvents are shown in the SI (Figures S13, S21, S25, S29, and S33). While ^{1}H NMR spectroscopy confirmed complete consumption of the norbornene

end group, SEC appeared to show only 94% MM conversion to BB polymer. We attribute this discrepancy to 6% of the MM sample that lacks the norbornene end group, as we have seen before in similar MMs.[42] We therefore adjusted all conversion values to account for this 6% residual PS MM. We also noticed that the experimental points fall slightly below the first order fit above ~60% conversion in all polymerizations. We attribute this decrease in k_p at moderate to high conversions to a small but observable dependence of k_p on N_{bb} in the growing BB polymer chain. This behavior is consistent with reports suggesting that steric hindrance near the chain end of the propagating species slows the propagation rate,[35] with the MM being hindered by the brush as it approaches the reactive chain end.[64] The results for each solvent at each purity level are shown in Figure 1B and Table S1, revealing several interesting and some unexpected results.

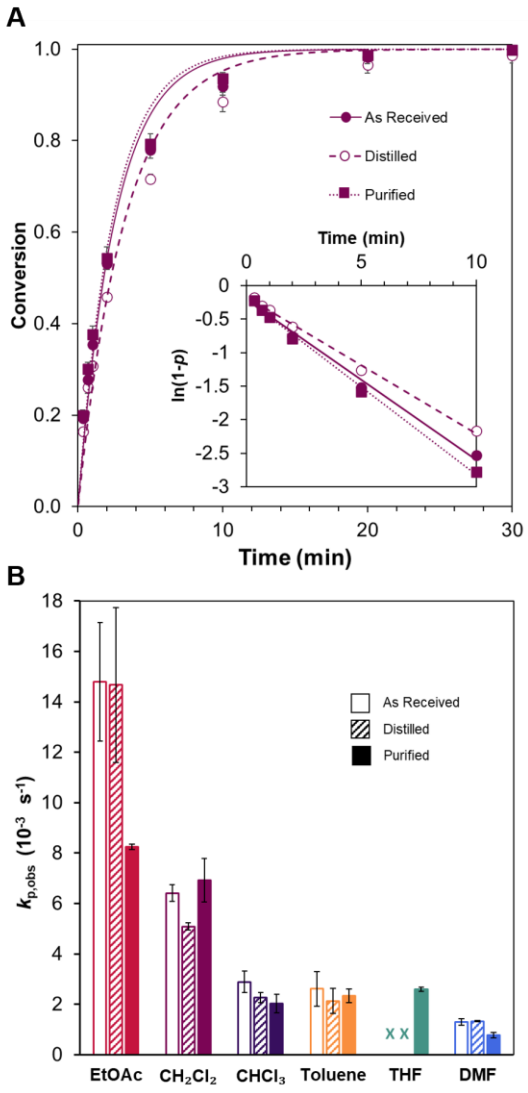

Figure 1. (A) Conversion versus time plot for ROMP of **PS$_{Br}$** MM in CH_2Cl_2 (50 mg/mL) at three different purity levels. Lines show first-order kinetics fits for each series. Error bars at each data point represent the standard deviation at each time point in 3–4 ROMP experiments for each purity category. Inset shows ln(1-p) versus time (p = MM conversion), where lines show first-order kinetics fits for each series. Similar plots for the other five solvents are shown in Figures S13, S21, S25, S29, and S33, and $k_{p,obs}$ and half-live values, MM conversion values, and polymer characterization results are shown in Table S1. (B) Measured first-order $k_{p,obs}$ values for ROMP of **PS$_{Br}$** in all six solvents with each different method of purification. Empty bars represent the as received solvents, lined bars represent distilled solvents, and solid bars represent purified solvents. The as received and distilled THF showed <3% conversion to BB polymer, so $k_{p,obs}$ could not be determined in these two cases. Error bars represent the standard deviation in 3–4 ROMP experiments for each solvent.

First, EtOAc, regardless of whether it was used as received, distilled, or more rigorously purified, led to the highest $k_{p,obs}$ among all solvents. CH_2Cl_2 was the next fastest solvent and polymerized **PS_{Br}** more than twice as fast as $CHCl_3$, toluene, and THF. DMF was the slowest solvent regardless of the purification method and was about 6-fold slower than EtOAc. Second, our hypothesis that $k_{p,obs}$ would increase with distillation or purification was disproven—the purified solvents mostly decreased or had little impact on $k_{p,obs}$. Purified EtOAc showed the most significant change in rate, with an almost 50% reduction in $k_{p,obs}$ after purification. We speculate that this could be due to the presence of acetic acid in as received EtOAc. Acetic acid likely protonates the labile pyridine ligands in G3, preventing them from re-binding to the active site on the Ru complex, allowing for faster MM addition, thus an increased polymerization rate. We experimentally tested this hypothesis by performing ROMP reactions in purified EtOAc spiked with 20 equiv acetic acid relative to catalyst (Figure S41) and found that k_p increased to a similar level to that of the as received EtOAc. Support for this conclusion comes from recent work by Guirronet and coworkers that showed that ROMP using G3 is -1 order in pyridine, meaning that k_p is inversely proportional to pyridine concentration.[63]

THF was an interesting case, as we saw little ROMP (less than 3% conversion) with the as received and distilled levels of purity. Purified THF was taken from solvent drying columns charged with activated alumina, and polymerization with THF from this source went to full conversion at a rate similar to $CHCl_3$ and toluene. We speculate that low levels of peroxides in as received and even in distilled uninhibited THF cause almost instantaneous catalyst decomposition, although we could not conclusively confirm this. However, rapid catalyst decomposition was obvious based on the change in the color of the G3 solution from green to brown upon dissolution

in as received or distilled THF; this color change did not occur with purified THF or any of the other solvents.

In the case of DMF, which was the slowest solvent in all cases, MM conversion values were lower (84–89%) compared with the other solvents (97–99%), and dispersity values were generally higher ($Đ$ = 1.2–1.4 for DMF, and ~1.1 for all other solvents). Interestingly, we observed a similar trend to EtOAc when comparing $k_{p,obs}$ values across solvents with different levels of purity, where purification actually reduced $k_{p,obs}$ by about 50%. Typical impurities in DMF include dimethylamine and formic acid,[65] so the enhanced rate of ROMP in the as received DMF (and even distilled DMF, where these impurities likely remain) may be attributed to the formic acid, which boils nearly 100 °C higher than dimethylamine so is likely present in higher concentrations than dimethylamine.

Finally, we note that these trends for as received solvents may depend on levels of impurities present in the as received forms, which may vary between suppliers and batches of solvents, causing variance in the rate of propagation.

Macromonomer and end group effects on ROMP propagation rate

We next asked whether the rate effects were similar when using different MMs or whether our observations were specific to PS MMs prepared by ATRP. Therefore, we synthesized two PnBA MMs using ATRP and photoiniferter polymerization with molecular weights similar to **PS$_{Br}$** (Scheme 1); these were named **PnBA$_{Br}$** and **PnBA$_{TTC}$**, where TTC indicates the trithiocarbonate end group. The goal in creating these two additional MMs was to determine whether the side chain chemistry (PS or PnBA) or side chain end group (Br or trithiocarbonate) affected $k_{p,obs}$. With these two additional MMs in hand, we again performed a series of ROMP reactions to measure $k_{p,obs}$ in

the six selected solvents, this time using only the purified solvents. Again, we targeted N_{bb} = 100 by conducting ROMP at a 100:1 MM:G3 ratio for each reaction. Aliquots were removed and analyzed by SEC, and first-order kinetics fits were determined using the same methods as used for **PS$_{Br}$**. A summary of results highlighting $k_{p,obs}$ values for **PS$_{Br}$**, **PnBA$_{Br}$**, and **PnBA$_{TTC}$** in each of the six purified solvents is shown in Figure 2.

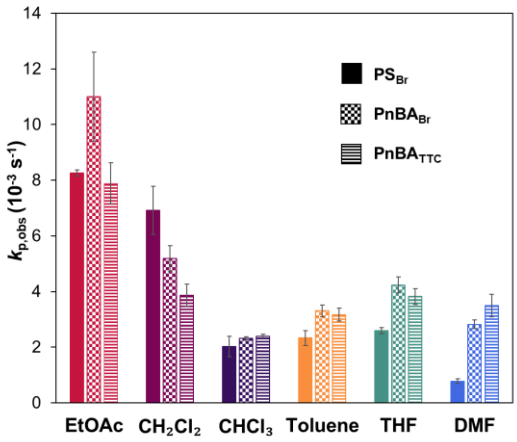

Figure 2. Measured $k_{p,obs}$ values based on first-order kinetics fits for the ROMP of **PS$_{Br}$** (filled bar), **PnBA$_{Br}$** (checked bar), and **PnBA$_{TTC}$** (lined bar) in purified solvents. Error bars represent the standard deviation in 3–4 ROMP experiments for each solvent.

Overall, changes to the polymer side chain and end groups caused only small perturbations in the $k_{p,obs}$ values. However, the PnBA side chains in **PnBA$_{Br}$** and **PnBA$_{TTC}$** reduced $k_{p,obs}$ by about 50% compared with **PS$_{Br}$** in CH_2Cl_2 and increased $k_{p,obs}$ about 4-fold compared with **PS$_{Br}$** in DMF. These two results may be associated with the behavior of the MM in the solvent, where PS has a less extended conformation in DMF than PnBA does, while the opposite effect occurs in CH_2Cl_2 (see below for further discussion). With these measurements regarding the effect of MM molecular structure on the relative rate of propagation for grafting-through ROMP, further investigations

were made into not only the differences in these two solvents as it relates to MMs, but also into the substantial difference between the propagation rate in the six different solvents.

We next set out to explain why k_p varied across the different solvents. Others have considered similar questions: For example, Grubbs and coworkers found that the initiation rate of G3 varied directly with the dielectric constant of the solvent,[28] and Matyjaszewski and coworkers discovered a relationship between the enthalpy of grafting-through ATRP reactions and the Hansen solubility parameters.[66] With this precedent established, we investigated numerous parameters describing the solvents themselves and compared them to the measured $k_{p,obs}$ values for **PS$_{Br}$** and **PnBA$_{TTC}$**. These parameters included solubility parameters, solvent dielectric constant, and the viscosity of each solvent (Figure S42). None of these properties showed a discernible relationship with the measured $k_{p,obs}$ values for **PS$_{Br}$**. We also compared the polymer-solvent interaction parameters for PS with each solvent to the $k_{p,obs}$ values and saw no correlation. Finally, we experimentally compared the polymer behavior in solution for each solvent. To do this, we performed static light scattering (SLS) experiments on high molecular weight linear PS (M_w = 200 kg/mol) and PnBA (M_w = 180 kg/mol) in each of the six pure solvents. We highlight the experimental methods and results of these experiments in the supporting information (Figure S43, Table S4, and Table S5). While we identified a possible relationship in the propagation rate decrease from PnBA to PS in DMF, there was no clear trend or conclusions for all of the solvents from these experiments.

Propagation rate of ROMP for a small molecule norbornene

In order to compare our results on MMs with a small molecule norbornene, we measured $k_{p,obs}$ values of *exo*-norbornene-5-methyl benzoate (**NMB**) in the same purified solvents (Scheme 2). In these experiments, we used a monomer concentration of 20 mM and targeted a backbone DP of

100. As in the kinetics experiments with the MMs, aliquots were taken at timepoints throughout the polymerization and added to vials containing EVE to terminate the reaction. The solvent was removed, and the conversion at each timepoint was determined using ^{1}H NMR spectroscopy by comparing the integral areas of the olefin proton peaks of the **NMB** to the olefin proton peaks of **poly(NMB)** (Figure S34). We initially found that polymerizations were too fast to measure effectively using our typical methods (half-lives were <5 s in several solvents). Therefore, we performed these studies with 10 equiv of added pyridine, which slowed the reaction enough to obtain measurable reaction rates. Figure 3A and Table S6 show the $k_{p,obs}$ values for each polymerization, while figures 3B-D compare **poly(NMB)** $k_{p,obs}$ values to the $k_{p,obs}$ values of the $\mathbf{PS_{Br}}$ (B), $\mathbf{PnBA_{Br}}$ (C), and the $\mathbf{PnBA_{TTC}}$ (D) MMs.

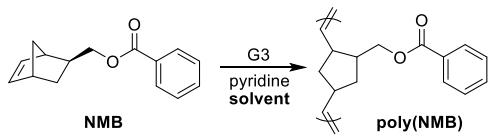

Scheme 2. ROMP of small molecule **NMB** used for comparison of $k_{p,obs}$ values with and without polymer pendant side chains.

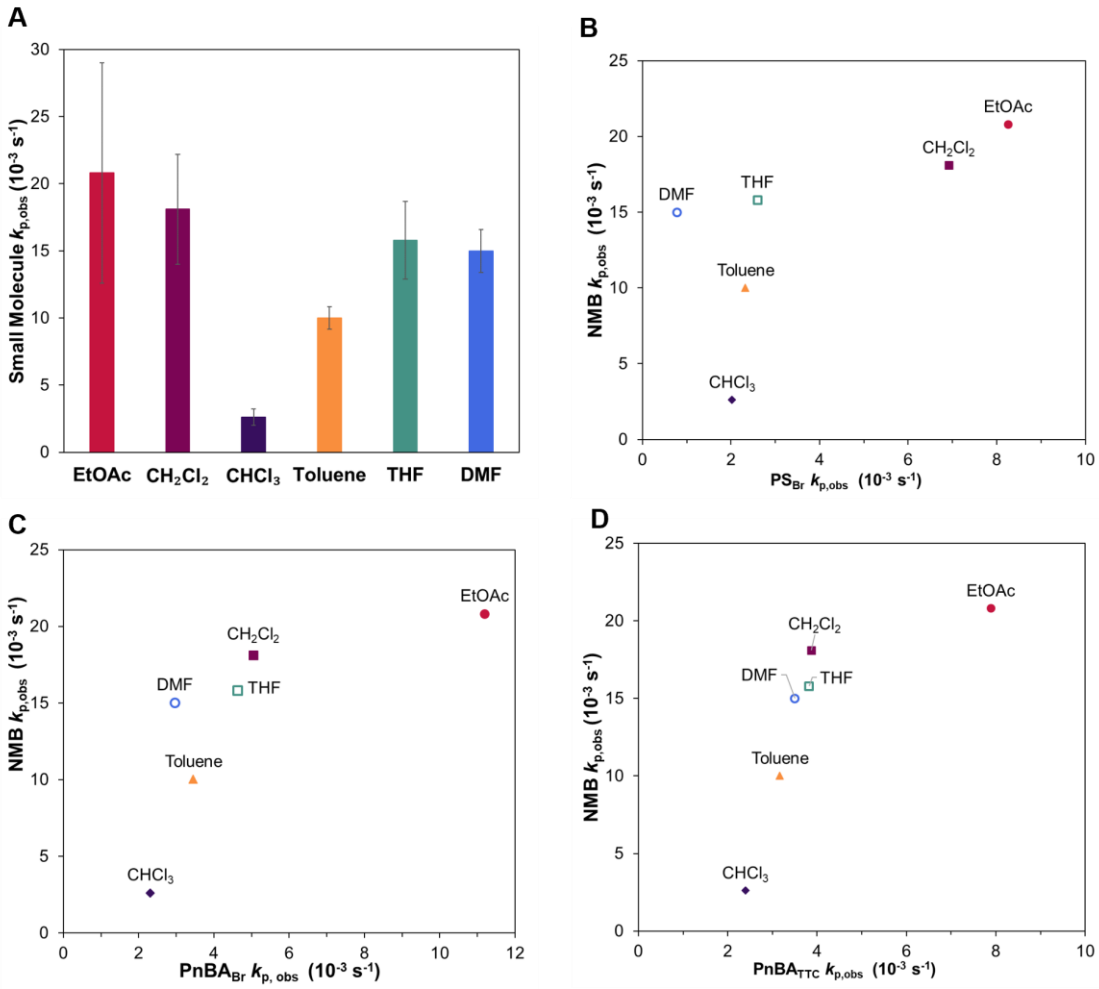

Figure 3. A) Graph showing $k_{p,obs}$ values for the ROMP of **NMB** in six purified solvents. The error bars represent the standard deviation in three independent experiments. B–D) Graphs comparing the **NMB** $k_{p,obs}$ to the MM $k_{p,obs}$ for B) **PS_{Br}**, C) **$PnBA_{Br}$**, and D) **$PnBA_{TTC}$**.

Figures 3B-D reveal that the $k_{p,obs}$ values for **NMB** and the three MMs show an approximately linear relationship in the different solvents (i.e., EtOAc has the highest rate for both **NMB** and the MMs). The $k_{p,obs}$ value in $CHCl_3$ for **NMB** was much lower than expected and substantially slower than the polymerizations performed in the other solvents. When adding pyridine to $CHCl_3$ prior to starting the reaction, we noticed the formation of an opaque solution. We believe this could be associated with a complexation between pyridine and $CHCl_3$,[67] which appears to hinder the activity of the G3 catalyst. The combined data provide evidence that ROMP propagation rate is more

affected by the activity and stability of the G3 catalyst in the particular solvent than it is by the nature or presence of a polymer pendant chain. While EtOAc and CH_2Cl_2 generally promoted faster ROMP propagation than other solvents, the differences are consistent between both **NMB** and the three MMs tested here. The differences in propagation rates are larger when using MMs versus a small molecule norbornene, highlighting the importance of solvent choice when making complex polymer topologies such as BB polymers using ROMP.

Rate of catalyst decomposition

To estimate the rate of catalyst decomposition, we explored the stability of the catalyst itself, without considering the MM or the ROMP grafting-through step. We used UV-Vis spectroscopy to monitor the decrease in the absorption of the metal-ligand charge transfer (MLCT) band associated with the Ru-benzylidene in G3, implying catalyst decomposition over time.[28,68] In these experiments, G3 was dissolved in each solvent at the same concentration as used during the ROMP kinetics experiments. We measured the absorbance change over time at the MLCT wavelength of 344 nm and fit the results to a first-order kinetics plot (Figure 4). We note that these decomposition experiments were not done in the presence of monomer because the catalyst spectrum becomes featureless after initiation. We also could not monitor decomposition in the presence MM by NMR spectroscopy because there is so little catalyst mass added with respect to MM that we could not see a benzylidene or alkylidene peak.

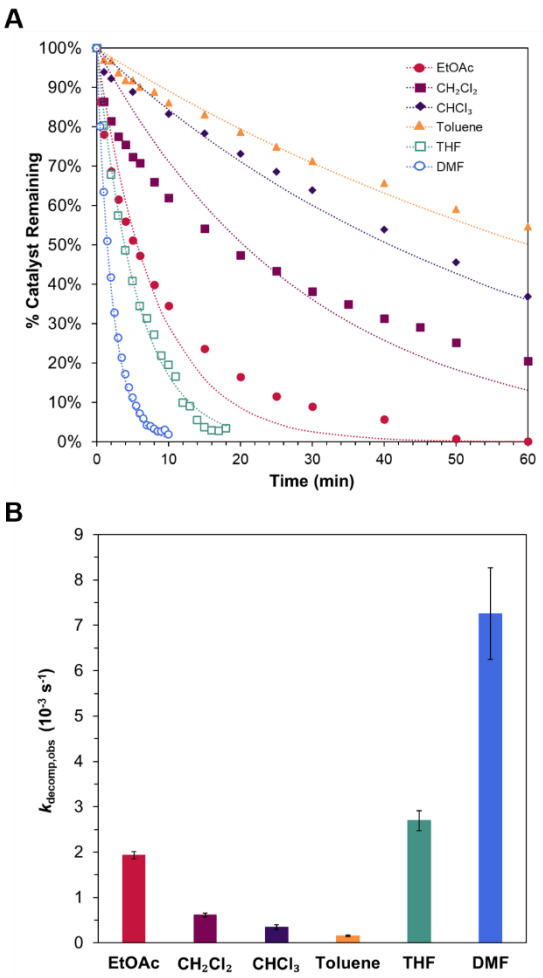

Figure 4. A) Change in % catalyst remaining over time in each solvent, as determined by monitoring absorbance of the MLCT peak (344 nm). Studies were performed in covered vessels under air with a concentration of 0.075 mg/mL G3 (0.10 mM) in solvent. B) Measured first-order rates of catalyst decomposition in each purified solvent in triplicate (Table S7). The error bars represent the standard deviation from three independent experiments.

While each solvent showed catalyst decomposition over time, toluene showed the slowest decomposition rate, while DMF and THF showed the fastest decomposition rates, with half-lives on the order of a few minutes. These rates were surprisingly fast considering that ROMP reactions on MMs in these solvents take longer than a few minutes, indicating that catalyst decomposition is slower in the presence of monomer than in its absence. These two solvents also showed the best fits to first-order kinetics, suggesting a single primary decomposition pathway in these solvents

and multiple pathways or higher-order processes in the other solvents. Fast decomposition in THF and DMF is consistent with work from Grubbs and coworkers comparing the rate of initiation of ruthenium olefin metathesis catalysts in different solvents.[28] They noted that the solvent dielectric constant was roughly proportional to the rate of initiation in various solvents. It is likely that these moderately polar, coordinating solvents interact with the catalyst in a way that favors decomposition pathways more than less polar solvents incapable of coordination. In our experiments, solvent dielectric constant did not vary linearly with our measured $k_{p,obs}$ values, but the theory behind why THF and DMF led to the fastest catalyst decomposition is still comparable to Grubbs's explanation of results: The state of the G3 ruthenium complex, when the catalyst has an available coordination site, is electron-deficient and could be available for coordination by more polar solvents (i.e., those with higher dielectric constants), which would inhibit the coordination of the monomer. Our results suggest that solvent coordination leads to faster decomposition. This also tracks with studies showing that less polar solvents generally favor productive olefin metathesis, while highly polar solvents instead promote higher levels of olefin isomerization and catalyst decomposition.[69] Finally, this conclusion is also supported by studies showing that some Ru catalysts have unusual decomposition pathways in solvents with high dielectric constants.[70]

In the case of EtOAc, which could presumably coordinate to the catalyst through its ester linkage, the decomposition rate aligns with previous reports;[28] however, the rate of propagation was much faster in EtOAc than in any other solvent. Future computational work may be able to shed some light on specific interactions between the catalyst and EtOAc that enhance catalytic activity. Another explanation for these results could be related to the behavior of the pyridines that are in equilibrium at the active site on the ruthenium complex.[63] If pyridine has higher solubility

in a specific solvent, it may drive the equilibrium toward the free pyridine and the active 14-electron catalyst species, enabling monomer binding to the active site.

Macromonomer conversion at high target N_{bb} values

Our ultimate goal in this work was to evaluate "livingness" in ROMP grafting-through in each of these solvents. A good method to assess "livingness" is to target a high DP to see if the targeted molecular weight can be reached at high monomer conversion levels while maintaining low $Đ$. Therefore, we prepared a new PS MM by ATRP with M_n = 3.0 kg/mol and subjected it to ROMP when targeting an N_{bb} of 1000 (instead of 100 as in the earlier experiments) in each purified solvent. The reactions were set up in a similar way to the kinetics experiments, but each polymerization was allowed to run for 24 h. After quenching the reaction, we used SEC to estimate the MM conversion to BB polymer in each polymerization by comparing the area of the BB polymer peak to the residual MM peak, both using the data obtained from the differential refractive index detector. We also compared expected molecular weight based on measured conversion values and a target N_{bb} = 1000 with observed molecular weight by SEC.

The results of the experiments are shown in Figure 5 and in Table S8. DMF and THF reached the lowest conversions, with less than 15% for both, while the other solvents reached >80% conversion. Toluene was the solvent that showed the lowest $k_{decomp,obs}$ when probing catalyst decomposition in each solvent, consistent with its ability in this experiment to achieve the highest conversion over a long reaction time (24 h). Observed and expected M_n values based on its 97% conversion were also quite close in toluene (2750 kg/mol versus 2820 kg/mol, respectively), and toluene was also the solvent leading to the BB polymer with the lowest $Đ$ of 1.44 ($Đ$ values between 1.47 and 1.60 were observed for the other solvents). Therefore, we conclude that toluene,

despite its relatively low $k_{p,obs}$, provided the most living system for this MM due to its very low $k_{decomp,obs}$. However, dispersity still suffered at this high targeted N_{bb} due to some catalyst decomposition. EtOAc, CH_2Cl_2, and $CHCl_3$ also reached high conversions (87%, 94%, and 81%, respectively), with M_n values also within 20% of expected values based on conversion. $Đ$ values for EtOAc, CH_2Cl_2, and $CHCl_3$ in this experiment were 1.55, 1.52, and 1.47, respectively. Therefore, these three solvents with the highest $k_{p,obs}$ values and relatively low $k_{decomp,obs}$ values also provide a relatively high degree of livingness (Figure S45). THF and DMF did not perform as well, with conversion values reaching 13% and 5%, respectively. Finally, we ran a similar experiment on a PnBA MM (M_n = 4.8 kg/mol), in this case targeting N_{bb}=500 due to the larger size of this MM. The results were similar to the PS MM, where toluene showed the highest conversion and M_n close to the expected value; EtOAc, CH_2Cl_2, and $CHCl_3$ showed somewhat lower conversions, and THF and DMF showed very little conversion (Figure S46, Table S9).

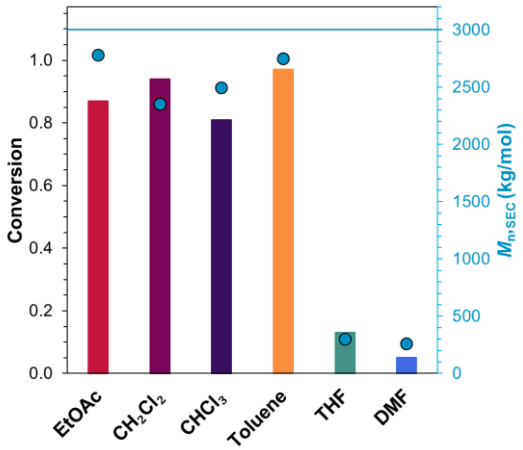

Figure 5. MM conversion to BB polymer (bars) and final BB polymer M_n (dots) in the grafting-through ROMP of **PS$_{Br}$** (3 kg/mol) in six purified solvents at a **PS$_{Br}$**/G3 ratio of 1000:1 (target N_{bb} = 1000) over 24 h. The horizontal bar represents the theoretical M_n at full conversion.

These results on high target N_{bb} values for both PS and PnBA MMs correlate with the catalyst decomposition results and suggest that catalyst decomposition plays the primary role in limiting

ultimate N_{bb} in DMF and THF. In other words, in the synthesis of BB polymers, the rate of catalyst decomposition plays a critical role, especially in THF and DMF, because it begins to approach the rate of propagation for even moderately sized MMs.

CONCLUSIONS

In this study, we observed the effects of solvent choice and purity on the rate of propagation and decomposition in ROMP. By measuring propagation kinetics of three MMs of similar molecular weights (**PS$_{Br}$**, **PnBA$_{Br}$**, and **PnBA$_{TTC}$**) and **NMB**, a small molecule norbornene, in multiple solvents and purities, we found that solvent choice heavily influences "livingness" in ROMP. Depending on impurities present in the solvent, purification can have either a positive or negative impact, or in some cases no impact at all, on the rate of ROMP propagation. This was particularly evident in the almost two-fold decrease in propagation rate for polymerizations performed in as received EtOAc compared to purified EtOAc, which has led to current studies in our group on how small molecule additives affect the rate of propagation in ROMP. We also measured a noticeable difference between the solvents themselves, whether purified or not, which we attribute to specific catalyst–solvent effects. This is supported by our observations of the same general trends in $k_{p,obs}$ in a small molecule norbornene (**NMB**) compared to the three MMs. The different MMs tested here revealed polymer effects in some cases, such as **PS$_{Br}$** having a lower $k_{p,obs}$ in DMF than in any of the other solvents, which could be attributed to the collapsed conformation of PS in DMF. We found that the catalyst decomposition rate plays the largest role in the ultimate conversion that can be achieved in a given solvent when targeting high N_{bb} values, where among purified solvents, toluene outperformed all other solvents with the highest conversion, lowest dispersity, and M_n matching the expected value, with EtOAc and CH_2Cl_2 not too far behind. Future studies on

additives may reveal better solvent/additive combinations, and systematic studies on ROMP in an air-free environment compared with polymerizations under air could reveal more insights.

Overall, these results have produced several important conclusions. 1) Solvent purification is unnecessary in most situations, unless the chosen solvent is THF, in which case purification through activated alumina is required. 2) Solvent choice impacts the rate of propagation; for example, $k_{p,obs}$ in EtOAc is 2–4 times faster than most other solvents tested for all three MMs and nearly an order of magnitude faster than DMF for PS MMs. 3) Among purified solvents, high "livingness" is best achieved with toluene, at least with these MMs, but EtOAc and CH_2Cl_2 also perform well and have higher $k_{p,obs}$ values than toluene. Together, these results will be useful for future efforts in ROMP, especially in the context of sterically demanding or otherwise challenging monomers, helping researchers select the best reaction conditions for achieving well-defined and low dispersity ROMP polymers.

ASSOCIATED CONTENT

Supporting Information

The following files are available free of charge.

NMR spectra, SEC traces, kinetics graphs, R_g values, catalyst decomposition data (PDF)

ACKNOWLEDGEMENTS

This work was supported by the Army Research Office (74464-CH-II) and a joint grant between the National Science Foundation and the Binational Science Foundation (DMR-2104602). We thank Prof. Michael Schulz for the use of the UV-Vis instrument, and Abby Chin, Zhao Li, and

Anna Steele, for critical reading of the manuscript. We also thank Dr. Dylan Walsh for thoughtful and helpful discussions, as well as the reviewers for their valuable suggestions. Any opinions, findings, and conclusions or recommendations expressed in this material are those of the authors and do not necessarily reflect the views of the funding agencies.

REFERENCES

(1) Bielawski, C. W.; Grubbs, R. H. Living Ring-Opening Metathesis Polymerization. *Prog. Polym. Sci.* **2007**, *32* (1), 1–29. https://doi.org/10.1016/j.progpolymsci.2006.08.006.

(2) Varlas, S.; Lawrenson, S. B.; Arkinstall, L. A.; O'Reilly, R. K.; Foster, J. C. Self-Assembled Nanostructures from Amphiphilic Block Copolymers Prepared via Ring-Opening Metathesis Polymerization (ROMP). *Prog. Polym. Sci.* **2020**, *107*, 101278. https://doi.org/10.1016/j.progpolymsci.2020.101278.

(3) Choi, T. L.; Grubbs, R. H. Controlled Living Ring-Opening-Metathesis Polymerization by a Fast-Initiating Ruthenium Catalyst. *Angew. Chemie - Int. Ed.* **2003**, *42* (15), 1743–1746. https://doi.org/10.1002/anie.200250632.

(4) Jenkins, A. D.; Stepto, R. F. T.; Kratochvíl, P.; Suter, U. W. Glossary of Basic Terms in Polymer Science (IUPAC Recommendations 1996). *Pure Appl. Chem.* **1996**, *68* (12), 2287–2311. https://doi.org/10.1351/pac199668122287.

(5) Takamizu, K.; Nomura, K. Synthesis of Oligo(Thiophene)-Coated Star-Shaped ROMP Polymers: Unique Emission Properties by the Precise Integration of Functionality. *J. Am. Chem. Soc.* **2012**, *134* (18), 7892–7895. https://doi.org/10.1021/ja301526v.

(6) Golder, M. R.; Nguyen, H. V. T.; Oldenhuis, N. J.; Grundler, J.; Park, E. J.; Johnson, J. A. Brush-First and ROMP-Out with Functional (Macro)Monomers: Method Development, Structural Investigations, and Applications of an Expanded Brush-Arm Star Polymer Platform. *Macromolecules* **2018**, *51* (23), 9861–9870. https://doi.org/10.1021/acs.macromol.8b01966.

(7) Saunders, R. S.; Cohen, R. E.; Wong, S. J.; Schrock, R. R. Synthesis of Amphiphilic Star Block Copolymers Using Ring-Opening Metathesis Polymerization. *Macromolecules* **1992**, *25*, 2055–2057.

(8) Matsumura, S.; Hlil, A. R.; Lepiller, C.; Gaudet, J.; Guay, D.; Shi, Z.; Holdcroft, S.; Hay, A. S. ROMP-NMP-ATRP Combination for the Preparation of 3-Miktoarm Star Terpolymer via Click Chemistry. *J. Polym. Sci. Part A Polym. Chem.* **2008**, *47*, 497–504.

(9) Gorodetskaya, I. A.; Choi, T. L.; Grubbs, R. H. Hyperbranched Macromolecules via Olefin Metathesis. *J. Am. Chem. Soc.* **2007**, *129* (42), 12672–12673.

https://doi.org/10.1021/ja0759040.

(10) Mathers, R. T.; Damodaran, K.; Rendos, M. G.; Lavrich, M. S. Functional Hyperbranched Polymers Using Ring-Opening Metathesis Polymerization of Dicyclopentadiene with Monoterpenes. *Macromolecules* **2009**, *42* (5), 1512–1518. https://doi.org/10.1021/ma802441t.

(11) Ding, L.; Lin, L.; Wang, C.; Qiu, J.; Zhu, Z. Facile Synthesis of Linear-Hyperbranched Polyphosphoesters via One-Pot Tandem ROMP and ADMET Polymerization and Their Transformation to Architecturally Defined Nanoparticles. *J. Polym. Sci. Part A Polym. Chem.* **2015**, *53* (8), 964–972. https://doi.org/10.1002/pola.27524.

(12) Tuten, B. T.; Chao, D.; Lyon, C. K.; Berda, E. B. Single-Chain Polymer Nanoparticles via Reversible Disulfide Bridges. *Polym. Chem.* **2012**, *3* (11), 3068–3071. https://doi.org/10.1039/c2py20308a.

(13) Chen, R.; Benware, S. J.; Cawthern, S. D.; Cole, J. P.; Lessard, J. J.; Crawford-Eng, I. M.; Saxena, R.; Berda, E. B. Assessing Structure/Property Relationships and Synthetic Protocols in the Fabrication of Poly(Oxanorbornene Imide) Single-Chain Nanoparticles. *Eur. Polym. J.* **2019**, *112* (November 2018), 206–213. https://doi.org/10.1016/j.eurpolymj.2018.12.046.

(14) Zhou, Y.; Qu, Y.; Yu, Q.; Chen, H.; Zhang, Z.; Zhu, X. Controlled Synthesis of Diverse Single-Chain Polymeric Nanoparticles Using Polymers Bearing Furan-Protected Maleimide Moieties. *Polym. Chem.* **2018**, *9* (23), 3238–3247. https://doi.org/10.1039/c8py00481a.

(15) Chae, C. G.; Yu, Y. G.; Seo, H. Bin; Kim, M. J.; Kishore, M. Y. L. N.; Lee, J. S. Molecular and Kinetic Design for the Expanded Control of Molecular Weights in the Ring-Opening Metathesis Polymerization of Norbornene-Substituted Polyhedral Oligomeric Silsesquioxanes. *Polym. Chem.* **2018**, *9* (42), 5179–5189. https://doi.org/10.1039/c8py00870a.

(16) Hahn, M. E.; Randolph, L. M.; Adamiak, L.; Thompson, M. P.; Gianneschi, N. C. Polymerization of a Peptide-Based Enzyme Substrate. *Chem. Commun.* **2013**, *49* (28), 2873–2875. https://doi.org/10.1039/c3cc40472b.

(17) Ahmetali, E.; Sen, P.; Süer, N. C.; Aksu, B.; Nyokong, T.; Eren, T.; Şener, M. K. Enhanced Light-Driven Antimicrobial Activity of Cationic Poly(Oxanorbornene)s by Phthalocyanine Incorporation into Polymer as Pendants. *Macromol. Chem. Phys.* **2020**, *221* (24), 1–14. https://doi.org/10.1002/macp.202000386.

(18) Alaboalirat, M.; Matson, J. B. Poly(β-Cyclodextrin) Prepared by Ring-Opening Metathesis Polymerization Enables Creation of Supramolecular Polymeric Networks. *ACS Macro Lett.* **2021**, *10* (12), 1460–1466. https://doi.org/10.1021/acsmacrolett.1c00590.

(19) Heroguez, V.; Breunig, S.; Gnanou, Y.; Fontanille, M. Synthesis of α-Norbornenylpoly(Ethylene Oxide) Macromonomers and Their Ring-Opening Metathesis Polymerization. *Macromolecules* **1996**, *29* (13).

(20) Allcock, H. R.; De Denus, C. R.; Prange, R.; Laredo, W. R. Synthesis of Norbornenyl Telechelic Polyphosphazenes and Ring-Opening Metathesis Polymerization Reactions. *Macromolecules* **2001**, *34* (9), 2757–2765. https://doi.org/10.1021/ma001686i.

(21) Jha, S.; Dutta, S.; Bowden, N. B. Synthesis of Ultralarge Molecular Weight Bottlebrush Polymers Using Grubbs' Catalysts. *Macromolecules* **2004**, *37* (12), 4365–4374. https://doi.org/10.1021/ma049647k.

(22) Adjiman, C. S.; Clarke, A. J.; Cooper, G.; Taylor, P. C. Solvents for Ring-Closing Metathesis Reactions. *Chem. Commun.* **2008**, No. 24, 2806–2808. https://doi.org/10.1039/b802921k.

(23) Gatti, M.; Vieille-Petit, L.; Luan, X.; Mariz, R.; Drinkel, E.; Linden, A.; Dorta, R. Impact of NHC Ligand Conformation and Solvent Concentration on the Ruthenium-Catalyzed Ring-Closing Metathesis Reaction. *J. Am. Chem. Soc.* **2009**, *131* (27), 9498–9499. https://doi.org/10.1021/ja903554v.

(24) De Brito Sá, É.; De Matos, J. M. E. Ring Closing Metathesis by Hoveyda-Grubbs Catalysts: A Theoretical Approach of Some Aspects of the Initiation Mechanism and the Influence of Solvent. *Inorganica Chim. Acta* **2015**, *426*, 20–28. https://doi.org/10.1016/j.ica.2014.11.007.

(25) Schulz, M. D.; Wagener, K. B. Solvent Effects in Alternating ADMET Polymerization. *ACS Macro Lett.* **2012**, *1* (4), 449–451. https://doi.org/10.1021/mz200236r.

(26) Neary, W. J.; Kennemur, J. G. Variable Temperature ROMP: Leveraging Low Ring Strain Thermodynamics To Achieve Well-Defined Polypentenamers. *Macromolecules* **2017**, *50*, 4935–4941. https://doi.org/10.1021/acs.macromol.7b01148.

(27) Cazalis, C.; Héroguez, V.; Fontanille, M. Polymerizability of Cycloalkenes in a Living Ring-Opening Metathesis Polymerization Initiated by Schrock Complexes, 1. Effect of the Solvent on the Polymerization Kinetics. *Macromol. Chem. Phys.* **2000**, *201* (8), 869–876. https://doi.org/10.1002/(sici)1521-3935(20000501)201:8<869::aid-macp869>3.0.co;2-z.

(28) Sanford, M. S.; Love, J. A.; Grubbs, R. H. Mechanism and Activity of Ruthenium Olefin Metathesis Catalysts. *J. Am. Chem. Soc.* **2001**, *123* (27), 6543–6554. https://doi.org/10.1021/ja010624k.

(29) Matos, J. M. E.; Lima-Neto, B. S. Benefits of Donor Solvents as Additive on ROMP of Norbornene Catalyzed by Amine Ru Complexes. *J. Mol. Catal. A Chem.* **2005**, *240*, 233–238. https://doi.org/10.1016/j.molcata.2005.07.003.

(30) Ashworth, I. W.; Nelson, D. J.; Percy, J. M. Solvent Effects on Grubbs' Pre-Catalyst Initiation Rates. *Dalt. Trans.* **2013**, *42* (2), 4110–4113. https://doi.org/10.1039/c2dt32441e.

(31) Al Samak, B.; Amir-Ebrahimi, V.; Corry, D. G.; Hamilton, J. G.; Rigby, S.; Rooney, J. J.; Thompson, J. M. Dramatic Solvent Effects on Ring-Opening Metathesis Polymerization of Cycloalkenes. *J. Mol. Catal. A Chem.* **2000**, *160* (1), 13–21. https://doi.org/10.1016/S1381-1169(00)00228-4.

(32) Matyjaszewski, K. Ranking Living Systems. *Macromolecules* **1993**, *26*, 1787–1788.

(33) Walsh, D. J.; Guironnet, D. Macromolecules with Programmable Shape, Size, and Chemistry. *Proc. Natl. Acad. Sci. U. S. A.* **2019**, *116* (5), 1538–1542. https://doi.org/10.1073/pnas.1817745116.

(34) Radzinski, S. C.; Foster, J. C.; Chapleski, Jr., R. C.; Troya, D.; Matson, J. B. Bottlebrush Polymer Synthesis by Ring-Opening Metathesis Polymerization: The Significance of the Anchor Group. *J. Am. Chem. Soc.* **2016**, *138*, 6998–7004. https://doi.org/10.1021/jacs.5b13317.

(35) Feast, W. J.; Gibson, V. C.; Johnson, A. F.; Khosravi, E.; Mohsin, M. A. Well-Defined Graft Copolymers via Coupled Living Anionic and Living Ring Opening Metathesis Polymerisation. *J. Mol. Catal. A Chem.* **1997**, *115* (1), 37–42. https://doi.org/10.1016/S1381-1169(96)00078-7.

(36) Breunig, S.; Heroguez, V.; Gnanou, Y.; Fontanille, M. Ring-Opening Metathesis Polymerizaton of w-Norbornenyl Polystyrene Macromonomers and Characterization of the Corresponding Structures. *Macromol. Symp.* **1995**, *95*, 151–166.

(37) Alaboalirat, M.; Qi, L.; Arrington, K. J.; Qian, S.; Keum, J. K.; Mei, H.; Littrell, K. C.; Sumpter, B. G.; Carrillo, J. Y.; Verduzco, R.; Matson, J. B. Amphiphilic Bottlebrush Block Copolymers: Analysis of Aqueous Self-Assembly by Small-Angle Neutron Scattering and Surface Tension Measurements. *Macromolecules* **2019**, *52*, 465–476. https://doi.org/10.1021/acs.macromol.8b02366.

(38) Liu, J.; Gao, A. X. iaod.; Johnson, J. A. Particles without a Box: Brush-First Synthesis of Photodegradable PEG Star Polymers under Ambient Conditions. *J. Vis. Exp.* **2013**, No. 80, 1–7. https://doi.org/10.3791/50874.

(39) Arrington, K. J.; Matson, J. B. Assembly of a Visible Light Photoreactor: An Inexpensive Tool for Bottlebrush Polymer Synthesis via Photoiniferter Polymerization. *Polym. Chem.* **2017**, *8*, 7452–7456. https://doi.org/10.1039/c7py01741c.

(40) Abd-El-Aziz, A. S.; Edel, A. L.; May, L. J.; Epp, K. M.; Hutton, H. M. Controlled Molecular Design of Ether- and Ester-Bridged Norbornenes and Their Ring-Opening Metathesis Polymerizations. *Can. J. Chem.* **1999**, *77* (11), 1797–1809. https://doi.org/10.1139/v99-164.

(41) Armarego, W. L. F.; Chai, C. L. L. C. *Purification of Laboratory Chemicals*, Sixth.; Elsevier Inc.: Oxford, UK, 2009.

(42) Radzinski, S. C.; Foster, J. C.; Scannelli, S. J.; Weaver, J. R.; Arrington, K. J.; Matson, J. B. Tapered Bottlebrush Polymers: Cone-Shaped Nanostructures by Sequential Addition of Macromonomers. *ACS Macro Lett.* **2017**, *6*, 1175–1179. https://doi.org/10.1021/acsmacrolett.7b00724.

(43) Verduzco, R.; Li, X.; Pesek, S. L.; Stein, G. E. Structure, Function, Self-Assembly, and Applications of Bottlebrush Copolymers. *Chem. Soc. Rev.* **2015**, *44*, 2405–2420.

https://doi.org/10.1039/c4cs00329b.

(44) Sheiko, S. S.; Sumerlin, B. S.; Matyjaszewski, K. Cylindrical Molecular Brushes: Synthesis, Characterization, and Properties. *Prog. Polym. Sci.* **2008**, *33*, 759–785. https://doi.org/10.1016/j.progpolymsci.2008.05.001.

(45) Johnson, J. A.; Lu, Y. Y.; Burts, A. O.; Xia, Y.; Durrell, A. C.; Tirrell, D. A.; Grubbs, R. H. Drug-Loaded, Bivalent-Bottle-Brush Polymers by Graft-through ROMP. *Macromolecules* **2010**, *43* (24), 10326–10335. https://doi.org/10.1021/ma1021506.

(46) Lv, F.; Liu, D.; Cong, H.; Shen, Y.; Yu, B. Synthesis, Self-Assembly and Drug Release Behaviors of a Bottlebrush Polymer-HCPT Prodrug for Tumor Chemotherapy. *Colloids Surfaces B Biointerfaces* **2019**, *181* (April), 278–284. https://doi.org/10.1016/j.colsurfb.2019.05.045.

(47) Vohidov, F.; Milling, L. E.; Chen, Q.; Zhang, W.; Bhagchandani, S.; Nguyen, H. V. T.; Irvine, D. J.; Johnson, J. A.; Johnson, J. A. ABC Triblock Bottlebrush Copolymer-Based Injectable Hydrogels: Design, Synthesis, and Application to Expanding the Therapeutic Index of Cancer Immunochemotherapy. *Chem. Sci.* **2020**, *11* (23), 5974–5986. https://doi.org/10.1039/d0sc02611e.

(48) Raj, W.; Jerczynski, K.; Rahimi, M.; Przekora, A.; Matyjaszewski, K.; Pietrasik, J. Molecular Bottlebrush with PH-Responsive Cleavable Bonds as a Unimolecular Vehicle for Anticancer Drug Delivery. *Mater. Sci. Eng. C* **2021**, *130* (August), 112439. https://doi.org/10.1016/j.msec.2021.112439.

(49) Liberman-Martin, A. L.; Chu, C. K.; Grubbs, R. H. Application of Bottlebrush Block Copolymers as Photonic Crystals. *Macromol. Rapid Commun.* **2017**, *38* (13), 1–15. https://doi.org/10.1002/marc.201700058.

(50) Chae, C. G.; Yu, Y. G.; Seo, H. Bin; Kim, M. J.; Grubbs, R. H.; Lee, J. S. Experimental Formulation of Photonic Crystal Properties for Hierarchically Self-Assembled POSS-Bottlebrush Block Copolymers. *Macromolecules* **2018**, *51* (9), 3458–3466. https://doi.org/10.1021/acs.macromol.8b00298.

(51) Boyle, B. M.; Collins, J. L.; Mensch, T. E.; Ryan, M. D.; Newell, B. S.; Miyake, G. M. Impact of Backbone Composition on Homopolymer Dynamics and Brush Block Copolymer Self-Assembly. *Polym. Chem.* **2020**, *11* (45), 7147–7158. https://doi.org/10.1039/d0py01007c.

(52) Li, Y.-L.; Chen, X.; Geng, H.-K.; Dong, Y.; Wang, B.; Ma, Z.; Pan, L.; Ma, G.-Q.; Song, D.-P.; Li, Y.-S. Oxidation Control of Bottlebrush Molecular Conformation for Producing Libraries of Photonic Structures. *Angew. Chemie - Int. Ed.* **2021**, *60*, 3647–3653.

(53) Li, X.; Shamsijazeyi, H.; Pesek, S. L.; Agrawal, A.; Hammouda, B.; Verduzco, R. Thermoresponsive PNIPAAM Bottlebrush Polymers with Tailored Side-Chain Length and End-Group Structure. *Soft Matter* **2014**, *10* (12), 2008–2015. https://doi.org/10.1039/c3sm52614c.

(54) Nam, J.; Kim, Y. J.; Kim, J. G.; Seo, M. Self-Assembly of Monolayer Vesicles via Backbone-Shiftable Synthesis of Janus Core-Shell Bottlebrush Polymer. *Macromolecules* **2019**, *52* (24), 9484–9494. https://doi.org/10.1021/acs.macromol.9b01429.

(55) Chowdhury, A. U.; Chang, D.; Xu, Y.; Hong, K.; Sumpter, B. G.; Carrillo, J. M. Y.; Doughty, B. Mapping the Interfacial Chemistry and Structure of Partially Fluorinated Bottlebrush Polymers and Their Linear Analogues. *Langmuir* **2021**, *37* (1), 211–218. https://doi.org/10.1021/acs.langmuir.0c02786.

(56) Rzayev, J. Molecular Bottlebrushes: New Opportunities in Nanomaterials Fabrication. *ACS Macro Lett.* **2012**, *1*, 1146–1149. https://doi.org/10.1021/mz300402x.

(57) Pang, X.; He, Y.; Jung, J.; Lin, Z. 1D Nanocrystals with Precisely Controlled Dimensions, Compositions, and Architectures. *Science (80-.).* **2016**, *353*, 1268–1272.

(58) Neugebauer, D.; Zhang, Y.; Pakula, T.; Sheiko, S. S.; Matyjaszewski, K. Densely-Grafted and Double-Grafted PEO Brushes via ATRP. A Route to Soft Elastomers. *Macromolecules* **2003**, *36* (18), 6746–6755. https://doi.org/10.1021/ma0345347.

(59) Daniel, W. F. M.; Burdyńska, J.; Vatankhah-varnoosfaderani, M.; Matyjaszewski, K.; Paturej, J.; Rubinstein, M.; Dobrynin, A. V; Sheiko, S. S. Solvent-Free , Supersoft and Superelastic Bottlebrush Melts and Networks. *Nat. Mater.* **2016**, *15*, 183–190. https://doi.org/10.1038/NMAT4508.

(60) Arrington, K. J.; Radzinski, S. C.; Drummey, K. J.; Long, T. E.; Matson, J. B. Reversibly Cross-Linkable Bottlebrush Polymers as Pressure-Sensitive Adhesives. *ACS Appl. Mater. Interfaces* **2018**, *10*, 26662–26668. https://doi.org/10.1021/acsami.8b08480.

(61) Walsh, D. J.; Dutta, S.; Sing, C. E.; Guironnet, D. Engineering of Molecular Geometry in Bottlebrush Polymers. *Macromolecules* **2019**, *52* (13), 4847–4857. https://doi.org/10.1021/acs.macromol.9b00845.

(62) Dutertre, F.; Bang, K.; Vereroudakis, E.; Loppinet, B.; Yang, S.; Kang, S.; Fytas, G.; Choi, T. Conformation of Tunable Nanocylinders : Up to Sixth-Generation Dendronized Polymers via Graft-Through Approach by ROMP. *Macromolecules* **2019**, *52*, 3342–3350. https://doi.org/10.1021/acs.macromol.9b00457.

(63) Walsh, D. J.; Lau, S. H.; Hyatt, M. G.; Guironnet, D. Kinetic Study of Living Ring-Opening Metathesis Polymerization with Third-Generation Grubbs Catalysts. *J. Am. Chem. Soc.* **2017**, *139*, 13644–13647. https://doi.org/10.1021/jacs.7b08010.

(64) Ren, N.; Yu, C.; Zhu, X. Topological Effect on Macromonomer Polymerization. *Macromolecules* **2021**, *54* (13), 6101–6108. https://doi.org/10.1021/acs.macromol.1c00256.

(65) Marsella, J. A. Dimethylformamide. *Kirk-Othmer Encyclopedia of Chemical Technology*. January 18, 2013, pp 1–9. https://doi.org/https://doi.org/10.1002/0471238961.0409130513011819.a01.pub2.

(66) Martinez, M. R.; Krys, P.; Sheiko, S. S.; Matyjaszewski, K. Poor Solvents Improve Yield

of Grafting-Through Radical Polymerization of OEO 19 MA. *ACS Macro Lett.* **2020**, *9*, 674–679. https://doi.org/10.1021/acsmacrolett.0c00245.

(67) Goldman, E.; Ragle, J. L. Complex of Pyridine with Chloroform: Deuterium Nuclear Quadrupole Coupling. *J. Phys. Chem.* **1986**, *90* (24), 6440–6446. https://doi.org/10.1021/j100282a008.

(68) Foster, J. C.; Grocott, M. C.; Arkinstall, L. A.; Varlas, S.; Redding, M. J.; Grayson, S. M.; O'Reilly, R. K. It Is Better with Salt: Aqueous Ring-Opening Metathesis Polymerization at Neutral PH. *J. Am. Chem. Soc.* **2020**. https://doi.org/10.1021/jacs.0c05499.

(69) Engel, J.; Smit, W.; Foscato, M.; Occhipinti, G.; Törnroos, K. W.; Jensen, V. R. Loss and Reformation of Ruthenium Alkylidene: Connecting Olefin Metathesis, Catalyst Deactivation, Regeneration, and Isomerization. *J. Am. Chem. Soc.* **2017**, *139* (46), 16609–16619. https://doi.org/10.1021/jacs.7b07694.

(70) Lynn, D. M.; Mohr, B.; Grubbs, R. H.; Henling, L. M.; Day, M. W. Water-Soluble Ruthenium Alkylidenes: Synthesis, Characterization, and Application to Olefin Metathesis in Protic Solvents. *J. Am. Chem. Soc.* **2000**, *122* (28), 6601–6609. https://doi.org/10.1021/ja0003167.

AUTHOR INFORMATION

Corresponding Author

*John B. Matson – Department of Chemistry and Macromolecules Innovation Institute, Virginia Tech, Blacksburg, VA, 24061, United States; orcid.org/0000-0001-7084-5396; Email: jbmatson@vt.edu

ORCID

Sarah E. Blosch: 0000-0002-3383-5771

John B. Matson: 0000-0001-7984-5396

Funding Sources

Any funds used to support the research of the manuscript should be placed here (per journal style).

Notes

The authors declare no competing financial interest.